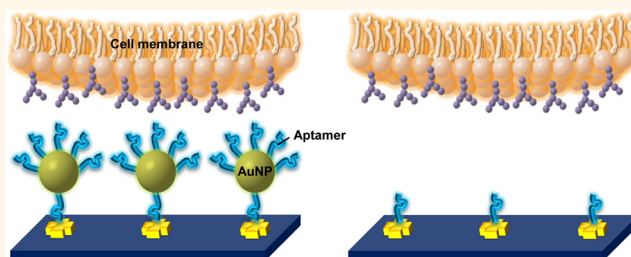# Multivalent DNA Nanospheres for Enhanced Capture of Cancer Cells in Microfluidic Devices

Weian Sheng,[†] Tao Chen,[‡] Weihong Tan,[‡,*] and Z. Hugh Fan[†,‡,§,*]

[†]Interdisciplinary Microsystems Group, Department of Mechanical and Aerospace Engineering, University of Florida, P.O. Box 116250, Gainesville, Florida 32611, United States , [‡]Department of Chemistry, University of Florida, P.O. Box 117200, Gainesville, Florida 32611, United States , and [§]J. Crayton Pruitt Family Department of Biomedical Engineering, University of Florida, P.O. Box 116131, Gainesville, Florida 32611, United States

ABSTRACT Isolation of circulating tumor cells (CTCs) from peripheral blood or cancer cells from bone marrow has significant applications in cancer diagnosis, therapy monitoring, and drug development. CTCs are cancer cells shed from primary tumors; they circulate in the bloodstream, leading to metastasis. The extraordinary rarity of CTCs in the bloodstream makes their isolation a significant technological challenge. Herein, we report the development of a platform combining multivalent DNA aptamer nanospheres with microfluidic devices for efficient isolation of cancer cells from blood. Gold nanoparticles (AuNPs) were used as an efficient platform for assembling a number of aptamers for high-efficiency cell capture. Up to 95 aptamers were attached onto each AuNP, resulting in enhanced molecular recognition capability. An increase of 39-fold in binding affinity was confirmed by flow cytometry for AuNP—aptamer conjugates (AuNP—aptamer) when compared with aptamer alone. With a laminar flow flat channel microfluidic device, the capture efficiency of human acute leukemia cells from a cell mixture in buffer increased from 49% using aptamer alone to 92% using AuNP—aptamer. We also employed AuNP—aptamer in a microfluidic device with herringbone mixing microstructures for isolation of leukemia cells in whole blood. The cell capture efficiency was also significantly increased with the AuNP—aptamer over aptamer alone, especially at high flow rates. Our results show that the platform combining DNA nanostructures with microfluidics has a great potential for sensitive isolation of CTCs and is promising for cancer diagnosis and prognosis.

The isolation of rare cells in peripheral blood such as circulating tumor cells (CTCs) is highly important but challenging.[1−3] CTCs are cancer cells shed from either primary tumors or metastatic sites and are highly related to the initiation of metastasis and the spread of cancer to distant organs. Thus CTCs hold the key for understanding metastasis, diagnosing cancer, and monitoring treatment response.[4−6] However, the extraordinary rarity of CTCs makes their isolation and characterization technically challenging. Traditionally, methods based on flow cytometry have been used in clinics, but with a considerable number of false negatives and low detection sensitivity.[7,8] The only FDA-approved CTC enumeration method is CellSearch Assay, which uses antibody-coated magnetic beads for CTC isolation. However, it suffers from low CTC-capture efficiency.[9,10] Recently, microfluidic devices with monovalent capture ligands, including antibodies[11−15] and nucleic acid aptamers,[16−18] have been extensively used for immunocapture of rare tumor cells. However, most efforts for increasing the sensitivity of cell capture are based on engineering complicated structures inside the microfluidic devices, such as microposts, sinusoidal channels, and silicon nanopillars, for enhancing ligand—cell interactions.[19−23] These structures make the device fabrication time-consuming and induce significant nonspecific cell capture, causing low specificity.
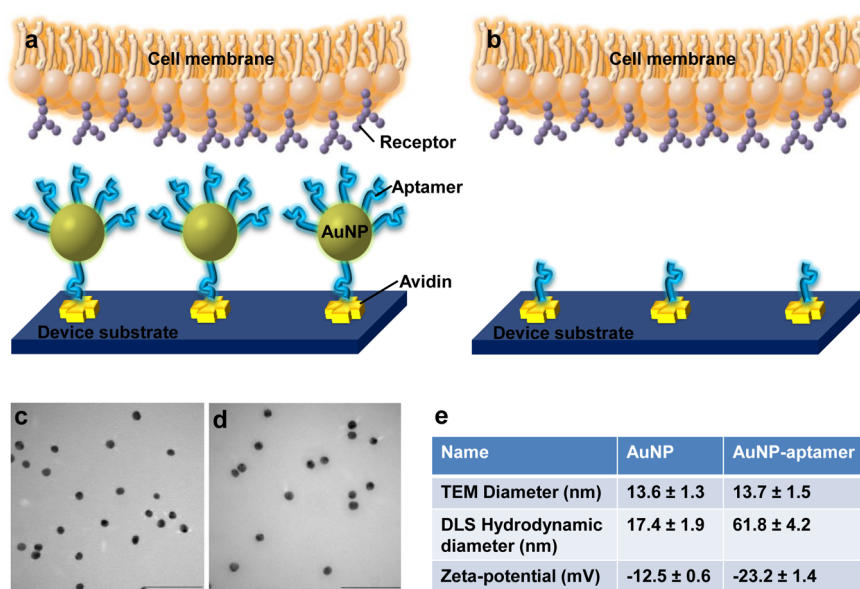
Herein, we have investigated the use of nanotechnology-based multivalent binding to enhance cell capture in microfluidic devices. Multivalent binding, the simultaneous interaction of multiple ligands on

Figure 1. (a, b) Illustration of enhanced cell capture using AuNP–aptamer-modified surface. With AuNP conjugation (a), multiple aptamers on the AuNP surfaces bind with multiple receptors on the cell membrane, leading to cooperative, multivalent interactions. Without AuNP (b), aptamer alone binds with receptors via monovalent interaction, with much fewer interactions. (c, d) Transmission electron microscopy (TEM) image of AuNPs (c) and AuNPs conjugated with aptamers (d); scale bar = 100 nm. (e) Comparison between AuNP and AuNP–aptamer in terms of particle diameters from TEM images, hydrodynamic diameters from dynamic light scattering (DLS) measurements, and zeta-potential measurements.

| Name	AuNP	AuNP-aptamer
TEM Diameter (nm)	13.6 ± 1.3	13.7 ± 1.5
DLS Hydrodynamic diameter (nm)	17.4 ± 1.9	61.8 ± 4.2
Zeta-potential (mV)	-12.5 ± 0.6	-23.2 ± 1.4

one entity with the complementary receptors on another, has been widely used for achieving high-affinity molecular recognition in biological processes.[24−28] The multivalency-enhanced binding between the ligands and targets in those biological systems has been extensively investigated.[29−31] To achieve multivalent binding, scaffolds from numerous nanoscale structures, such as dendrimers,[32,33] nanorods,[34] nanoparticles,[35] polymers,[36] and proteins, have been used by researchers for assembling multiple ligands, and dendrimer-mediated multivalent binding has been used for enhanced surface capture of cells.[33] Recently, nucleic acid aptamers have been selected for targeting numerous cancers,[37,38] and nanomaterial–aptamer conjugates have been extensively used for enhanced molecular recognition, but none of them have been used for enhancing capture of cancer cells.[39−43] Here, we hypothesize that the nanoparticle–aptamer conjugates could greatly improve the efficiency of capturing cancer cells. We chose gold nanoparticles (AuNPs) as the multivalent ligand scaffolds to assemble multiple DNA aptamers (DNA nanospheres) owing to their easy synthesis and conjugation with DNA.[44,45] Our flow cytometric analysis demonstrated the multivalent binding between aptamers and cells through AuNP conjugation. Then we developed a flat channel microfluidic device that is able to capture cancer cells from buffer or lysed blood with high efficiency and high throughput using the AuNP–aptamer conjugates (AuNP–aptamer). The enhanced binding affinity afforded by the AuNP–aptamer-modified surface significantly increased the capture efficiency of target cancer cells, and the AuNP–aptamer maintained

high capture efficiency with increased flow rate, which considerably improved the sample throughput of the microfluidic device.

The scheme of the AuNP–aptamer-mediated cell capture is shown in Figure 1. The microfluidic device surface is first coated with avidin by physical adsorption.[16,18] Then, biotinylated aptamer-conjugated AuNPs are immobilized onto the channel through biotin–avidin interaction. When a sample containing target cancer cells passes through the channel, cells are captured via the specific interaction between the aptamers and the target cell receptors. Since each AuNP is conjugated with ~95 aptamers, we hypothesize that the AuNP–aptamer binds to cell surface markers in a cooperative manner, leading to a multivalent effect and resulting in enhanced cell capture efficiency. Besides the multivalent binding, the AuNP–aptamer-modified surface increases the surface roughness[23] and allows enhanced local topographic interactions between the AuNP–aptamers and nanoscale receptors on the cell surface,[21,46,47] contributing to the increased cell capture.

RESULTS AND DISCUSSION

Synthesis and Characterization of AuNP–Aptamer Conjugates. AuNPs were prepared following the methods detailed in the Methods section. Figure 1c shows the transmission electron microscopy (TEM) image of the AuNPs, with an average diameter of 13.6 nm. The as-prepared AuNPs were then functionalized with thiol-modified DNA aptamers, and the TEM image is shown in Figure 1d, with an average size of 13.7 nm. A 24-unit polyethylene glycol (PEG) spacer between the AuNP
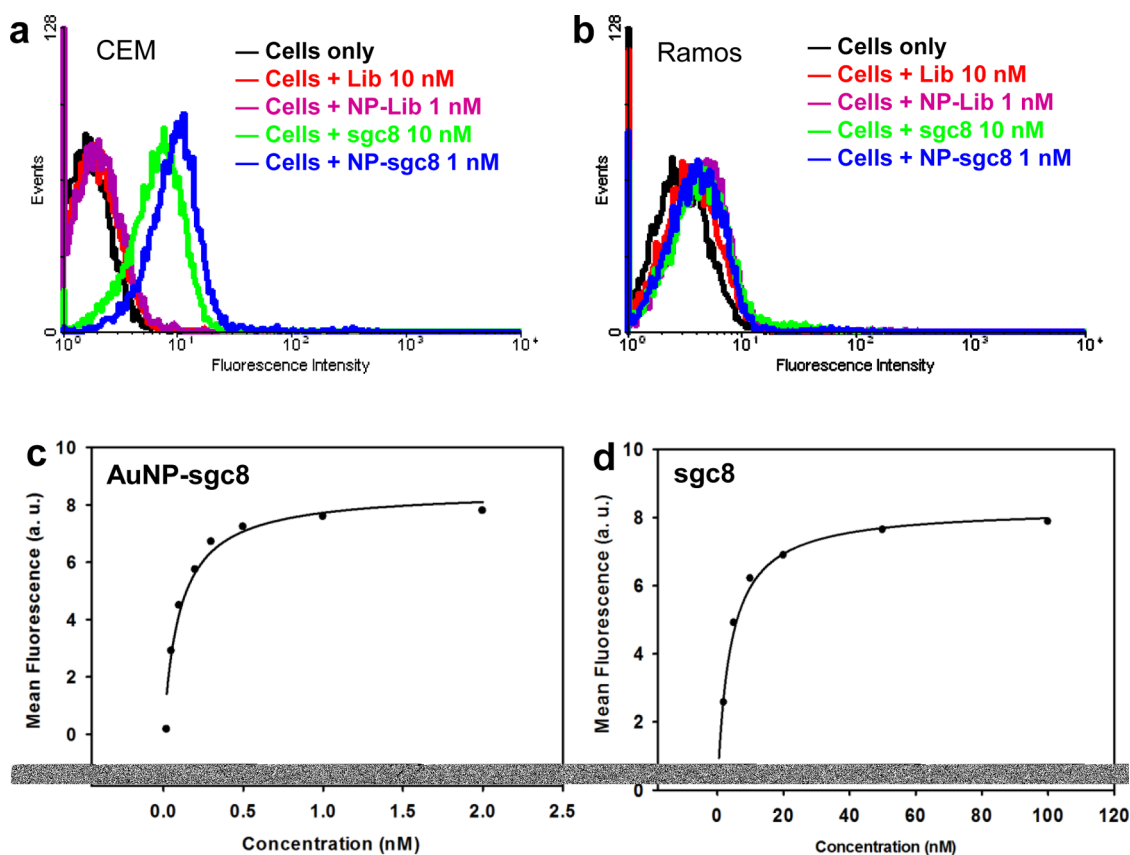
Figure 2. Flow cytometry shows the strong and specific binding of AuNP−sgc8 aptamer conjugates (AuNP−sgc8) with target CEM cells. (a) CEM cells selectively bind with free sgc8 and AuNP−sgc8 aptamers; negligible signal change was observed for cells incubated with random DNA library (Lib) or AuNP−Lib conjugates (NP−Lib) compared with cells only. (b) Control Ramos cells did not bind with either AuNP−sgc8 or sgc8 alone (with no signal shift for either case), demonstrating the specificity of free sgc8 and AuNP−sgc8 aptamers to CEM cells. (c, d) Flow cytometry analysis determines the binding affinity of AuNP−sgc8 (c) and sgc8 alone (d) to CEM cells.

surface and the aptamers was added to minimize the steric effects of the particle surface on the aptamers and to increase the loading of DNA on AuNPs.[48] Figure 1c and d show that the properties of AuNPs remained unchanged after conjugation with aptamers, without any aggregation. Dynamic light scattering (DLS) measurements showed that the hydrodynamic diameter of AuNPs was 17.4 nm. After conjugation with aptamers, the hydrodynamic diameter increased to 61.8 nm, demonstrating the successful conjugation of aptamers onto AuNPs (Figure S1 in the Supporting Information). Zeta-potential measurements indicated that the AuNPs had a zeta-potential of −12.5 mV. After modification with aptamers, the zeta-potential became −23.2 mV, which is attributed to the negative charges carried by DNA aptamers. The comparison of properties between AuNPs and AuNP−aptamers is made in Figure 1e.

Flow Cytometric Analysis Demonstrating High-Affinity Binding. To investigate the AuNP−aptamer-mediated multivalent binding, we directly measured the binding behaviors of AuNP−sgc8 aptamer conjugates (AuNP−sgc8) and free sgc8 aptamer (sgc8) using flow cytometry. Sgc8 is an aptamer that has specific binding with CEM cells (human acute lymphoblastic leukemia), with a nanomolar (nM)

dissociation constant (K_d).[37] Ramos cells (human Burkitt's lymphoma), which do not bind with sgc8 aptamer, were used as control cells here. Figure 2a shows a noticeable increase in fluorescence signal for both AuNP−sgc8 and free sgc8 aptamer compared to the random DNA library (Lib) and AuNP−Lib, proving that both have strong binding with their target cells. Besides, AuNP−sgc8 produces a higher fluorescence signal than free sgc8, even with 10 times lower concentration. As shown in Figure 2b, neither free sgc8 nor AuNP−sgc8 shows a signal increase when incubated with control Ramos cells, demonstrating the specificity of both free aptamers and AuNP−aptamers. Furthermore, the binding affinity of sgc8 and AuNP−sgc8 to CEM cells was measured quantitatively by studying their binding with varying concentrations of sgc8 and AuNP−sgc8 aptamers. As demonstrated in Figure 2c and d, AuNP−sgc8 shows a 39 times higher binding affinity ($K_d = 0.10 \pm 0.02$ nM) than that of free sgc8 ($K_d = 3.9 \pm 0.5$ nM). The lower dissociation constant of AuNP−sgc8 suggests a multivalent-mediated enhancement in binding affinity when multiple aptamers on the AuNP surface bind to multiple receptors on the cell membrane.

**Enhanced Cancer Cell Capture in a Flat Channel Microdevice.** To study the cancer cell capture using AuNP−aptamer,
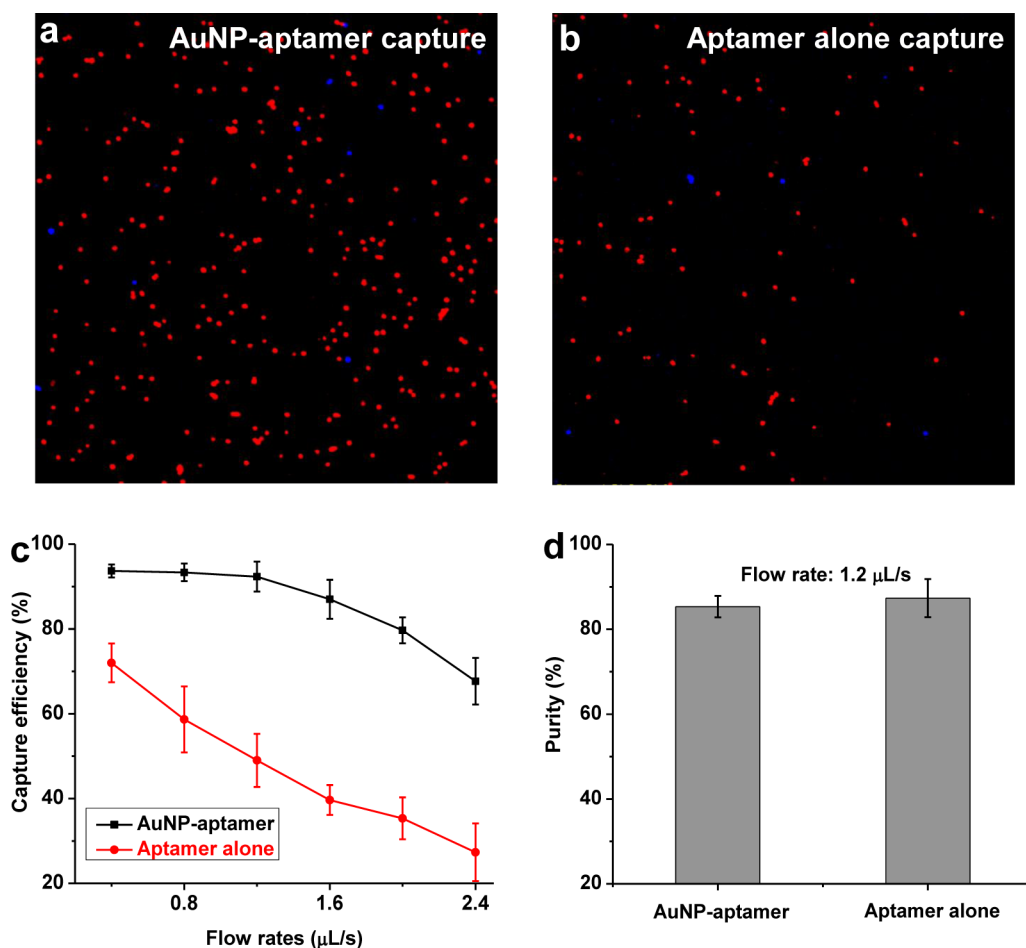
Figure 3. (a, b) Representative image of the target CEM cells (red) and control Ramos cells (blue) captured in the flat channel device using (a) AuNP–sgc8 aptamer conjugates and (b) sgc8 aptamer alone. Cell suspensions were continuously pumped into the device without interruption. (c) Comparison of CEM cell capture efficiency in PBS between AuNP–aptamer and aptamer alone when they were coated in a flat channel device, at flow rates from 0.4 to 2.4 μL/s. (d) Comparison of the capture purity of target CEM cells between AuNP–aptamer and aptamer alone at the same flow rate; no significant difference was observed. Error bars represent standard deviations (n = 3).

we first developed a microfluidic laminar flow device with flat channels (Figure S2b), which allowed us to directly compare the capture performance between AuNP–aptamer and aptamer alone. After coating surfaces with AuNP–sgc8 aptamer, a cell mixture containing 10^5 target CEM cells and 10^6 control Ramos cells (1:10 ratio) in 1 mL of phosphate-buffered saline (PBS) was introduced into the channel. Note that the cell solution was continuously pumped into the device without any interruption. CEM and Ramos cells were prestained with Vybrant DiI (red) and DiD (blue), respectively. Figure 3a shows a representative image of cells captured using AuNP–aptamer: a high percentage of target CEM cells (red) were captured, while most control Ramos cells (blue) were washed away. In another set of experiments with the same conditions, sgc8 alone was used instead of AuNP–sgc8. Figure 3b shows a typical image of cells captured after washing using aptamer alone (without the nanoparticle conjugation). The results in Figure 3a and b clearly indicate that much more target CEM cells were captured using AuNP–aptamer

than with aptamer alone, demonstrating that enhanced cell capture was achieved by the AuNP conjugation. The capture efficiency using AuNP–aptamer and aptamer alone was also studied at different flow rate conditions (with different shear stresses). We found that AuNP–aptamer exhibited more enhancement in capture efficiency at higher flow rates, as shown in Figure 3c. At a flow rate of 1.2 μL/s, AuNP–aptamer maintained a capture efficiency of (92 ± 4)%, while aptamer alone yielded a capture efficiency of only (49 ± 6)%. The capture efficiency was defined as the ratio of the number of target cells captured to the number of target cells initially seeded. The AuNP–aptamer enables significant increase in capture efficiency for the target cells. We also studied the purity of the captured cells and found that the capture purity is not affected by the AuNP conjugation. The purity was defined as the ratio of the number of target cells captured to the number of total cells captured. As shown in Figure 3d, similar purity was obtained for AuNP–aptamer and aptamer alone when the same flow rate was used; this suggests that AuNP–aptamer
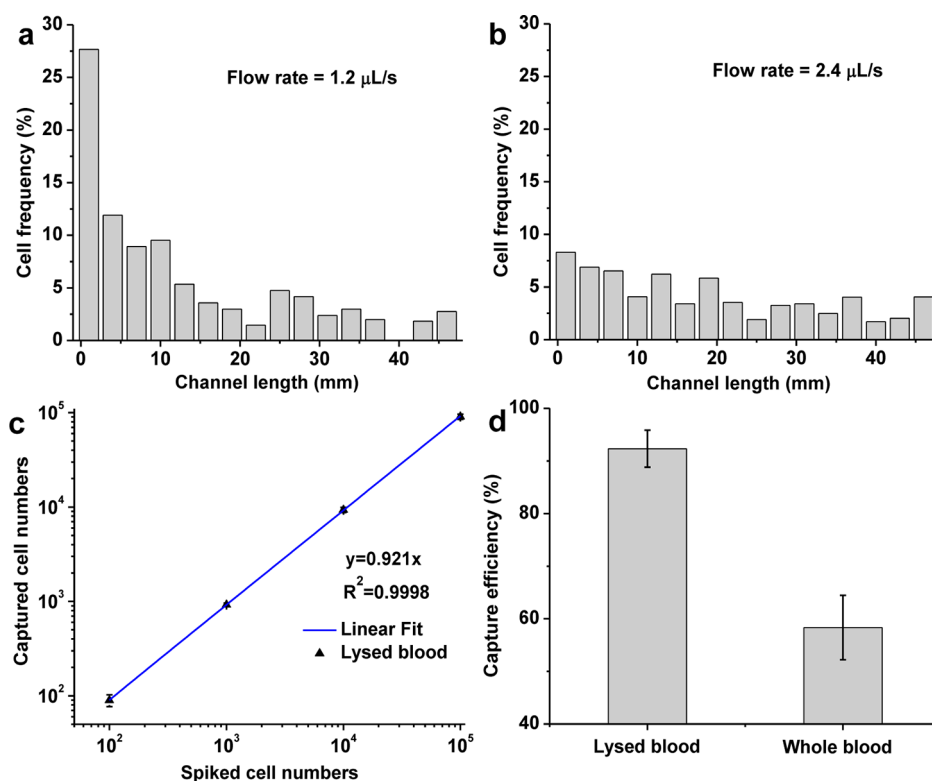
Figure 4. (a, b) Spatial distribution of surface-captured CEM cells along the 50 mm long microchannel in the flat channel device at different flow rates of (a) 1.2 μL/s and (b) 2.4 μL/s. (c) Capture efficiency for 100 000, 10 000, 1000, and 100 CEM cells spiked in 1 mL of lysed blood, with a flow rate of 1.2 μL/s. (d) CEM cell capture efficiency from lysed blood or whole blood at the same flow rate (1.2 μL/s); 1000 CEM cells were spiked in 1 mL of lysed blood or whole blood. Error bars represent the standard deviations of triplicate experiments.

does not introduce more nonspecific binding relative to aptamer alone, which is consistent with flow cytometry results in Figure 2b. However, the AuNP—aptamer allows us to use higher flow rates to maintain the capture efficiency. Higher purity can thus be obtained because nonspecifically adsorbed cells are more easily washed away with a stronger shear force at a higher flow rate.[18] Figure S3 demonstrates that the purity of captured cells was improved by the increasing flow rates with proportionally increased shear stresses.

In addition to the DNA nanosphere-mediated multivalent binding, the enhanced cell capture also accrues from the nanosphere-modified surface. The increases in the surface roughness and total surface area compared with the plain surface allowed enhanced local topographic interactions between the aptamer-coated nanoparticle and nanoscale components on the cell surface.[46] Moreover, the nanoparticle surfaces packed the aptamers in a highly dense manner, accommodating more aptamers to be immobilized than a plain surface, which is an additional advantage of using AuNP—aptamer. The increased ligand density also contributes to the enhanced interaction between cells and aptamers. Furthermore, the enhanced binding strength afforded by the multivalency effect lowers the detachment ratio of immobilized cells, thus increasing the capture efficiency compared to aptamer

alone. To evaluate the versatility of our system, we also applied the system for capturing Ramos cells using AuNP—TD05 aptamer conjugates. TD05 is an aptamer with specific binding to Ramos cells.[49] A capture efficiency of 90% was obtained with AuNP—TD05, while TD05 aptamer alone yielded only 41% capture, showing significant enhancement in capture efficiency as a result of using DNA nanospheres.

The reduced capture efficiency at higher flow rates (shown in Figure 3c) is due to increased flow-induced shear stress and the decreased interaction time between cells and aptamers on surfaces. We further characterized the distribution of captured cells at different locations of the 50 mm long microchannel with different flow rates. As shown in Figure 4a, at a flow rate of 1.2 μL/s (with a shear stress of 0.4 dyn/cm^2), 65% of the cells were captured in the first 25% of the channel coated with AuNP—aptamer. With an increased flow rate of 2.4 μL/s (Figure 4b), the cells captured were distributed along the channel because cells needed a longer flow distance (travel length) to have an opportunity to interact with aptamers coated on the surfaces, and the attached cells experienced proportionally increased shear stresses. The cell—surface interaction is due to the ligand—receptor binding as well as gravitational force. With the AuNP conjugation, the PEG spacer extends the aptamer strands into the 3D space of
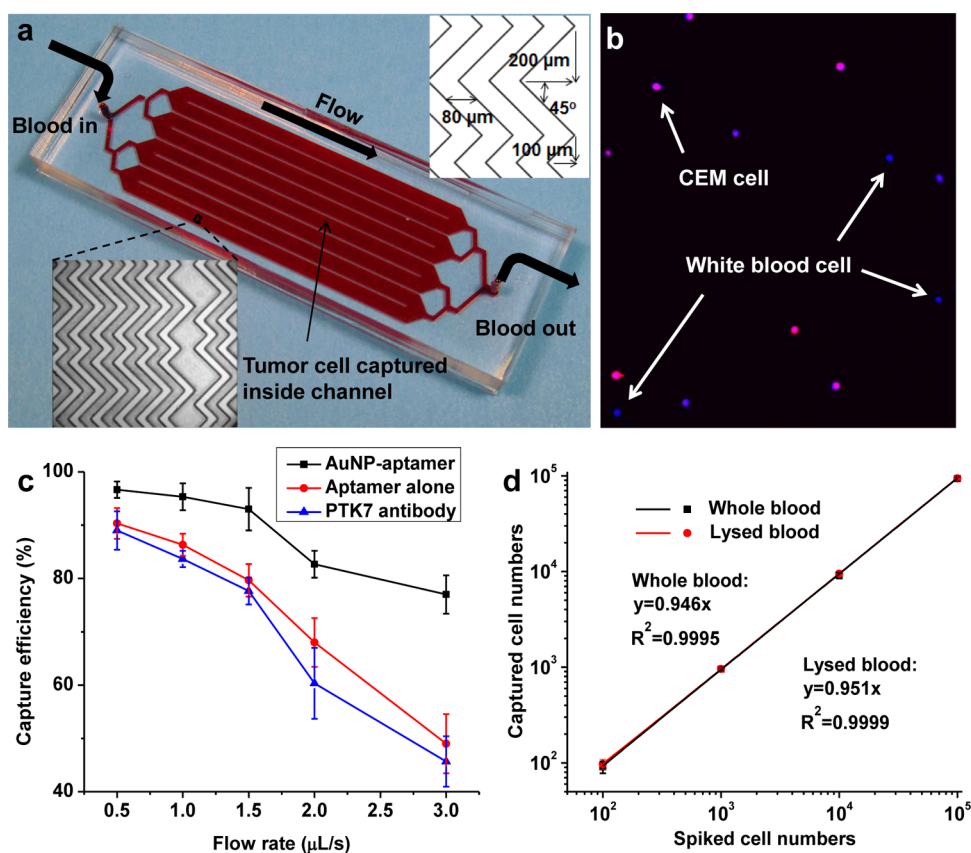
Figure 5. (a) Device layout and dimensions of a microfluidic device containing herringbone mixers. (b) Representative image of captured CEM cells (DiI+, DAPI+) from whole blood; the DAPI+ cells (blue only) are nonspecifically captured white blood cells. (c) CEM cell capture efficiency in whole blood at various flow rates using AuNP−aptamer, aptamer alone, and anti-PTK7 antibody, respectively. (d) Calibration plot of cancer cell capture from whole blood and lysed blood with different cell concentrations at 1.5 μL/s; solid lines represent linear fitting. Error bars represent standard deviations ($n = 3$).

the flow, increasing the accessibility and frequency of interactions between aptamers and cells to permit more efficient cell capture under higher flow rates.

To explore the clinical utility of the system, we assessed the isolation of CEM cells from lysed blood (blood with red blood cells lysed) at concentrations ranging from 10^5 to 100 cells/mL. As shown in Figure 4c, as few as 100 cells were efficiently isolated from 1 mL of lysed blood within 14 min. However, when we tried to capture cancer cells from unprocessed whole blood directly, the capture was significantly lower (even at a low flow rate), as shown in Figure 4d. The relatively low capture was primarily due to the reduced interaction chances between target cells and AuNP−aptamer, which is caused by abundant red blood cell blockage.

Efficient Isolation of Cancer Cells from Whole Blood Using DNA Nanospheres in Micromixer Devices. Although the laminar flow flat channel device achieved high efficiency when capturing cells in PBS or lysed blood, it showed a low capture efficiency (<60%) when capturing cells from whole blood. To enable the efficient capture of CTCs from whole blood, we integrated the AuNP−aptamer system into a herringbone groove-based micromixer device (Figure 5a). The staggered herringbone

mixer generates a microvortex and chaotic mixing inside the microchannel, which significantly enhances the cell−surface interactions, leading to higher capture efficiency.[12,22,50] We first evaluated the isolation of 10^4 CEM cells (prestained by DiI, red) spiked in 1 mL of whole blood at a flow rate of 1 μL/s. After cell capture and rinsing, 4,6-diamidino-2-phenylindole (DAPI) was introduced into the device to test the purity of the target cells. DAPI stained all the cancer cells and leukocytes with a blue color and verified that captured cells retain intact nuclei. As shown in Figure 5b, cells positive to both DAPI and DiI were target CEM cells (blue merged with red), while cells positive to DAPI only were white blood cells (blue only). A purity of $(70 \pm 6)\%$ was obtained when capturing CEM cells from whole blood, with a capture efficiency of $(95 \pm 3)\%$. This capture purity from whole blood is much higher than those reported in the literature (∼50% and 14%).[11,12] Further, we tested the capture efficiency over a wide range of flow rates from 0.5 to 3 μL/s. Control experiments using identical devices and conditions with aptamer alone (no AuNP conjugation) were then conducted. Much higher capture efficiencies were obtained using AuNP−aptamer than aptamer alone, especially at high flow rates (Figure 5c). The

combined effect of high-affinity binding from the AuNP—aptamer with the passive mixing provided by the herringbone structures enabled a high capture efficiency from whole blood (93%) at a high flow rate (1.5 μL/s). To compare the AuNP—aptamer-based cell capture with traditional antibody-based cell capture, protein tyrosine kinase 7 (PTK7) antibody was used for capturing CEM cells with identical device and conditions. For the binding between CEM cells and sgc8 aptamer, our previous study identified PTK7 as the marker for CEM cells.[51] As shown in Figure 5c, the capture efficiency of CEM cells using anti-PTK7 is comparable with aptamer alone, but significantly less than AuNP—aptamer. To test the limit of detection for the AuNP—aptamer-based cell capture system, cell spike numbers from 10^5 to 100 were explored, and >90% capture efficiency was obtained for all cases at the flow rate of 1.5 μL/s. Regardless of whether the red blood cells are intact or lysed, high capture efficiency is always obtained by the integration of AuNP—aptamer with a herringbone mixer (Figure 5d). In addition, with a flow rate of 1.5 μL/s (5.4 mL/h), 1 mL of blood sample can be processed in 11 min, which gives sufficient throughput for clinical applications. The system gives more benefit at higher flow rates and maintains a target cell capture efficiency of >75% for all flow rates up to 3 μL/s. With this flow rate, only 42 min is needed for processing 7.5 mL of blood, the amount of blood needed to detect a clinically relevant CTC number. Compared with reported work, this AuNP—aptamer-modified mixer device enables >90% capture at a flow rate of 5.4 mL/h, 2- to 4-fold higher than the reported aptamer-alone-based micropillar device (2.2 mL/h)[18] and antibody-coated herringbone device (1.2 mL/h).[12] The results show that the AuNP—aptamer-modified herringbone device has great potential for clinical CTC isolation and enumeration.

CONCLUSIONS

In summary, we demonstrated the use of gold nanoparticles as an efficient high-affinity vehicle for molecular assembly of aptamers for target cancer cell capture in microfluidic devices. Up to 95 aptamers were attached onto each AuNP, resulting in enhanced aptamer molecular recognition capability. Flow cytometry results demonstrated the high-affinity binding effect using AuNP—aptamer conjugates. The capture efficiency for target cancer cells was significantly increased using the AuNP—aptamer conjugates because of the cooperative, multiple ligand—receptor interactions, as well as the increased surface roughness and ligand density. With the AuNP—aptamer surface immobilization, a flat channel microfluidic device was able to capture 100 cancer cells from 1 mL of lysed blood with ∼90% capture efficiency within 14 min (4.3 mL blood/h). Using the integration of the AuNP—aptamer with a herringbone mixer design, efficient capture of rare cancer cells from whole blood was achieved, with a throughput of processing 1 mL of blood in 11 min. The high efficiency, throughput, and purity make the system suitable for clinical isolation of CTCs from patient blood.

The use of leukemia cell-targeting aptamers allows the platform to be suitable for minimal residual disease (MRD) detection. MRD is the small amount of leukemia cells remaining in patient blood during or after treatment when the patient is in remission, which is the major cause of cancer relapse.[52,53] Our system, capable of efficient isolation of rare cells, is suitable for sensitive detection of MRD, which will be promising for monitoring treatment response and predicting cancer relapse. However, aptamers are currently not as widely used as antibodies, and limited numbers of aptamers have been developed for targeting CTCs in patient blood. Our future efforts will include incorporating AuNPs with CTC-marker-binding aptamers [*e.g.*, anti-EpCAM aptamer (epithelial cell adhesion molecule),[54] anti-PSMA aptamer (prostate-specific membrane antigen)][55] for capturing CTCs from cancer patients, as well as exploring the release and culture of captured CTCs.

Spherical DNA nanostructures have been well developed and widely used for cancer cell detection; however, to our knowledge, this is the first use of aptamer nanospheres for enhancing cancer cell capture. Our results show that the combination of nanotechnology with a microfluidic device[56] has great potential for the sensitive isolation of cancer cells from patient blood and is promising for cancer diagnosis and monitoring treatment response.

METHODS

Synthesis and Characterization of Gold Nanoparticle—Aptamer Conjugates. Hydrogen tetrachloroaurate(III) (HAuCl$_4$), trisodium citrate dihydrate, tris(2-carboxyethyl)phosphine hydrochloride (TCEP), tris(hydroxymethyl)aminomethane (Tris), and sodium acetate were obtained from Sigma-Aldrich (St. Louis, MO, USA). Acetate buffer (500 mM, pH 5.2) was prepared using a mixture of sodium acetate and acetic acid. Tris acetate buffer (500 mM, pH 8.2) was prepared using Tris and acetic acid.

AuNPs were prepared using the protocols reported previously.[57] Briefly, 100 mL of 1 mM HAuCl$_4$ solution was heated to reflux. Then, 10 mL of 38.8 mM sodium citrate was added, and reflux was continued for another 20 min. The diameter of such prepared AuNPs was ∼13 nm, measured by transmission electron microscopy (TEM). The concentration of the AuNPs was ∼13 nM, determined by UV—vis measurement at 520 nm using a Cary Bio-300 UV spectrometer (Varian) (Figure S4).

DNA aptamers were synthesized in-house. The thiol-modified sgc8 aptamer sequence was 5'-thiol- PEG-ATC TAA CTG CTG CGC CGC CGG GAA AAT ACT GTA CGG TTA GA-biotin-3'. The sequences of all aptamers used are listed in Table S1. For flow cytometric analysis, a fluorescein isothiocyanate (FITC) modifier was used to replace the biotin linker. All DNA aptamers were purified using a ProStar HPLC (Varian, Walnut Creek, CA, USA)

with a C_{18} column (Econosil, 5U, 250 × 4.6 mm) from Alltech Associates (Deerfield, IL, USA), with triethylammonium acetate—acetonitrile as eluent. DNA concentration was determined by UV—vis measurement at 260 nm.

Thiol-modified aptamers were conjugated on AuNPs using the reported protocols.[48,57,58] Aptamers (9 μL, 1 mM) were added with acetate buffer (1 μL, 500 mM) and TCEP (1.5 μL, 10 mM) and incubated for 1 h at room temperature to activate the thiol group. Then the TCEP-treated aptamer was added to 3 mL of as-prepared AuNPs and incubated for 16 h. Finally, Tris acetate buffer (30 μL, 500 mM) and NaCl (300 μL, 1M) were added, and the mixture was incubated for 24 h. Unconjugated aptamers were then removed by centrifugation at 14 000 rpm for 15 min.

The aptamer concentration in the supernatant was measured, and the final conjugated aptamer concentration in the AuNPs was determined by subtracting the supernatant concentration from the previous aptamer concentration. The final AuNP concentration was 12.7 nM with an aptamer concentration of 1.2 μM, giving an average of approximately 95 aptamers on each AuNP. Dynamic light scattering measurement was performed to evaluate the hydrodynamic diameter of the AuNPs before and after conjugation with aptamers using a Zetasizer Nano ZS (Malvern, Worcestershire, United Kingdom) (Figure S1). Zeta-potential measurements were performed using the same instrument. Fluorescence spectroscopy (Figure S5) also demonstrated the successful conjugation of aptamer on the AuNP. The fluorescence signal of each AuNP—aptamer conjugate is much higher than that of an individual aptamer.

Device Design and Fabrication. A single flat channel device was initially used for proof-of-concept studies, and then eight flat channels were parallelized to form a high-throughput device. As shown in Figure S2a, the single flat channel device was designed with a length of 50 mm, a width of 2 mm, a depth of 100 μm, and a single inlet and outlet. Three independent devices can be incorporated within one microscope slide size (3 in. × 1 in.). To increase the throughput, eight channels were connected through parallelization, and uniform flow was maintained in the eight channels. The size of the high-throughput device is also 3 in. × 1 in., as shown in Figure S2b. Both of the devices were made of polydimethylsiloxane (PDMS) and bonded to a 3 in. × 1 in. glass slide.

PDMS devices were fabricated according to the procedures reported by Whitesides' group.[59] The layout of the device was designed in AutoCAD and then sent to CAD/Art Services, Inc. (Bandon, OR, USA) to produce a high-resolution transparency photomask. Silicon wafers (Silicon Inc., Boise, ID, USA) were first spin-coated with SU-8 2035 photoresist (MicroChem, Newton, MA, USA) using a spin coater (Laurell Tech., North Wales, PA, USA). Then the pattern on the photomask was transferred to the silicon substrate via UV exposure. After development, a silicon master patterned with the complementary structures was obtained. PDMS devices were fabricated by casting a liquid PDMS precursor against the master using Sylgard 184 reagents (Dow Corning, Midland, MI, USA) according to the instructions of the manufacturer. To prevent the cured PDMS from sticking to the silicon master, TFOCS (tridecafluoro-1,1,2,2-tetrahydrooctyl-1-trichlorosilane) (Sigma-Aldrich) was vacuum vaporized to the surface of the master. The channel depth, which was controlled by the spin speed of the SU-8, was measured using a Dektak 150 profilometer. The PDMS substrate was then sealed with a glass microscope slide, and inlet and outlet wells were created at the channel ends by punching holes in the PDMS sheet.

The design of the herringbone mixer device was inspired by several works in the literature,[12,50] and the dimensions were chosen for optimal cell capture, as shown in Figure 5a. The mixer device was fabricated as described above, but using a two-layer SU-8 fabrication technique, with one coating and exposure steps and a single developing step.[60] The silicon mold consists of a first layer as the main channel and the second layer as the herringbone ridges, which become grooves after transfer to the PDMS substrate.

Cell Lines and Buffers. T-cell human acute lymphoblastic leukemia cells (CCRF-CEM cells, CCL-119) and B-cell human

Burkitt's lymphoma cells (Ramos cells, CRL-1596) were purchased from American Type Culture Collection (ATCC). CEM and Ramos cells were cultured in RPMI medium 1640 (ATCC) supplemented with 10% fetal bovine serum (FBS; heat-inactivated; Gibco) and 100 units/mL penicillin—streptomycin (Cellgro, Manassas, VA, USA). Both cultures were incubated at 37 °C under a 5% CO_2 atmosphere. Dulbecco's phosphate-buffered saline with calcium and magnesium (PBS) (Fisher Scientific, Hampton, NH, USA) was used to wash cells. A solution of 50 mg/mL (5%) bovine serum albumin (BSA) (Fisher) and 0.1% Tween-20 (Fisher) in PBS was used for rinsing the unbound molecules on the surface and resuspending cells for the cell capture. BSA and Tween-20 in PBS can fully passivate the surfaces to reduce nonspecific adsorption of cells in the channel.

Flow Cytometric Analysis. Flow cytometry was used to evaluate the targeting capabilities of AuNP—aptamer conjugates toward specific cells. Fluorescence measurements were made with a FACScan cytometer (BD Immunocytometry Systems, San Jose, CA, USA). Briefly, 200 000 cells were incubated with FITC-labeled free aptamer or AuNP—aptamer conjugates in 200 μL of PBS (containing 0.1% BSA) for 30 min on ice. After incubation, the cells were washed three times by centrifugation with 200 μL of PBS, and 10 000 counts were measured in the flow cytometer to determine the fluorescence. Varying concentrations of free sgc8 and AuNP—sgc8 aptamers were used to determine their binding affinities. The FITC-labeled random DNA library was used as a negative control to determine nonspecific binding. All of the experiments for the binding assay were repeated three times. The mean fluorescence intensity of target cells labeled by aptamers was used to calculate the specific binding by subtracting the mean fluorescence intensity of nonspecific binding from the random DNA library.[37] The equilibrium dissociation constants (K_d) of the aptamer—cell interaction were obtained by fitting the dependence of fluorescence intensity of specific binding on the concentration of the aptamers to the equation $Y = B_{max}X/(K_d + X)$ using SigmaPlot (Jandel, San Rafael, CA, USA), where Y is the fluorescence intensity and X is the concentration of aptamers.

Cell Capture Assay in Microfluidic Devices. Immediately before cell capture experiments, cells were washed with PBS and resuspended at 10^6 cells/mL. By following the manufacturer's instructions, CEM and Ramos cells were stained with Vybrant DiI (red) and DiD (blue) cell-labeling solutions (Invitrogen, Carlsbad, CA, USA), respectively, then washed with PBS, and resuspended at 10^7 cells/mL in the PBS containing BSA and Tween-20. Labeled cells were stored on ice and further diluted to the desired concentrations before cell capture.

The single donor human whole blood was obtained from Innovative Research (Novi, MI, USA), with the anticoagulant ethylenediaminetetraacetic acid (EDTA). Lysed blood was obtained by treating whole blood with red blood cell lysing buffer (Sigma-Aldrich) (containing NH_4Cl) according to the manufacturer's instructions. Different concentrations of CEM cells were then spiked in whole blood or lysed blood.

To start the cell capture experiments, one device volume (~100 μL) of 1 mg/mL avidin (Invitrogen) in PBS was first introduced into the device, followed by incubation for 15 min and then three rinses with PBS. Then, 100 μL of sgc8 aptamer or AuNP—sgc8 aptamer was introduced into the device and incubated for 15 min, followed by three rinses with the PBS containing BSA and Tween-20. Finally, 1 mL of cell mixture or blood sample spiked with cancer cells was continuously pumped into the device at a flow rate of 1.2 μL/s (or other flow rates specified in the text). For cell capture using antibody, anti-PTK7 biotin (Miltenyi Biotec, Auburn, CA, USA) was used instead of sgc8 or AuNP—sgc8 aptamer. Afterward, the device was washed three times with PBS to remove nonspecifically captured cells, followed by acquiring fluorescent images to determine the cell numbers. To test the purity of captured cells from lysed blood or whole blood, DAPI (Invitrogen) was introduced into the device to label the nonspecifically captured white blood cells. By following the manufacturer's instructions, 300 nM DAPI was incubated with cells for 10 min, followed by rinsing with PBS.

The cell suspensions or blood samples were introduced into the device by pumping.[18] A Micro4 syringe pump (World

Precision Instruments, Sarasota, FL, USA) with a 1 mL syringe was connected to the inlet of the device *via* polymer tubing and a female luer-to-barb adapter (IDEX Health & Science, Oak Harbor, WA, USA). To avoid cell settling, a tiny magnetic stirring bar was placed inside the 1 mL syringe, with a stir plate beneath the syringe. The magnetic stirring bar kept cells in suspension while the cell mixture or blood was being pumped through the device. The device was placed on the stage of an Olympus IX71 fluorescence microscope (Olympus America, Melville, NY, USA) for detecting captured cells. To determine cell numbers, sets of images corresponding to the red fluorescent cells, blue fluorescent cells, and transmission images were acquired at different positions in each channel. Images were then imported into ImageJ (NIH), and cell counts were obtained using the Analyze Particles function after setting an appropriate threshold. Cell counts were further confirmed by comparing fluorescent images with transmission images; only those with appropriate cell morphology in the transmission images were counted.

Conflict of Interest: The authors declare no competing financial interest.

Supporting Information Available: DLS measurements of AuNPs and AuNP—aptamers, picture of flat channel microfluidic devices, purity of CEM cells as a function of flow rate, adsorption spectrum of AuNPs, fluorescence spectrum of fluorescein-labeled free aptamers and AuNP—aptamers, and table of aptamer sequences. This material is available free of charge via the Internet at http://pubs.acs.org.

REFERENCES AND NOTES

1. Kling, J. Beyond counting tumor cells. *Nat. Biotechnol.* **2012**, *30*, 578–580.
2. Yu, M.; Stott, S.; Toner, M.; Maheswaran, S.; Haber, D. A. Circulating tumor cells: approaches to isolation and characterization. *J. Cell Biol.* **2011**, *192*, 373–382.
3. Galanzha, E. I.; Shashkov, E. V.; Kelly, T.; Kim, J.-W.; Yang, L.; Zharov, V. P. In vivo magnetic enrichment and multiplex photoacoustic detection of circulating tumour cells. *Nat. Nanotechnol.* **2009**, *4*, 855–860.
4. Pantel, K.; Brakenhoff, R. H.; Brandt, B. Detection, clinical relevance and specific biological properties of disseminating tumour cells. *Nat. Rev. Cancer* **2008**, *8*, 329–340.
5. Cristofanilli, M.; Budd, G. T.; Ellis, M. J.; Stopeck, A.; Matera, J.; Miller, M. C.; Reuben, J. M.; Doyle, G. V.; Allard, W. J.; Terstappen, L. W. M. M.; *et al*. Circulating tumor cells, disease progression, and survival in metastatic breast cancer. *N. Engl. J. Med.* **2004**, *351*, 781–791.
6. Danila, D. C.; Fleisher, M.; Scher, H. I. Circulating tumor cells as biomarkers in prostate cancer. *Clin. Cancer Res.* **2011**, *17*, 3903–3912.
7. He, W.; Wang, H.; Hartmann, L. C.; Cheng, J.-X.; Low, P. S. In vivo quantitation of rare circulating tumor cells by multiphoton intravital flow cytometry. *Proc. Natl. Acad. Sci.* **2007**, *104*, 11760–11765.
8. Issadore, D.; Chung, J.; Shao, H.; Liong, M.; Ghazani, A. A.; Castro, C. M.; Weissleder, R.; Lee, H. Ultrasensitive clinical enumeration of rare cells ex vivo using a micro-Hall detector. *Sci. Transl. Med.* **2012**, *4*, 141ra92.
9. Riethdorf, S.; Fritsche, H.; Müller, V.; Rau, T.; Schindlbeck, C.; Rack, B.; Janni, W.; Coith, C.; Beck, K.; Jänicke, F.; *et al*. Detection of circulating tumor cells in peripheral blood of patients with metastatic breast cancer: a validation study of the CellSearch System. *Clin. Cancer Res.* **2007**, *13*, 920–928.
10. Balic, M.; Williams, A.; Lin, H.; Datar, R.; Cote, R. J. Circulating tumor cells: from bench to bedside. *Annu. Rev. Med.* **2013**, *64*, 31–44.
11. Nagrath, S.; Sequist, L. V.; Maheswaran, S.; Bell, D. W.; Irimia, D.; Ulkus, L.; Smith, M. R.; Kwak, E. L.; Digumarthy, S.; Muzikansky, A.; *et al*. Isolation of rare circulating tumour cells in cancer patients by microchip technology. *Nature* **2007**, *450*, 1235–U10.
12. Stott, S. L.; Hsu, C. H.; Tsukrov, D. I.; Yu, M.; Miyamoto, D. T.; Waltman, B. A.; Rothenberg, S. M.; Shah, A. M.; Smas, M. E.; Korir, G. K.; *et al*. Isolation of circulating tumor cells using a microvortex-generating herringbone-chip. *Proc. Natl. Acad. Sci. U.S.A.* **2010**, *107*, 18392–18397.
13. Ozkumur, E.; Shah, A. M.; Ciciliano, J. C.; Emmink, B. L.; Miyamoto, D. T.; Brachtel, E.; Yu, M.; Chen, P.-i.; Morgan, B.; Trautwein, J.; *et al*. Inertial focusing for tumor antigen-dependent and -independent sorting of rare circulating tumor cells. *Sci. Transl. Med.* **2013**, *5*, 179ra47.
14. Schiro, P. G.; Zhao, M.; Kuo, J. S.; Koehler, K. M.; Sabath, D. E.; Chiu, D. T. Sensitive and high-throughput isolation of rare cells from peripheral blood with ensemble-decision aliquot ranking. *Angew. Chem., Int. Ed.* **2012**, *51*, 4618–4622.
15. Zheng, X.; Cheung, L. S.-L.; Schroeder, J. A.; Jiang, L.; Zohar, Y. A high-performance microsystem for isolating circulating tumor cells. *Lab Chip* **2011**, *11*, 3269–3276.
16. Phillips, J. A.; Xu, Y.; Xia, Z.; Fan, Z. H.; Tan, W. Enrichment of cancer cells using aptamers immobilized on a microfluidic channel. *Anal. Chem.* **2009**, *81*, 1033–1039.
17. Xu, Y.; Phillips, J. A.; Yan, J.; Li, Q.; Fan, Z. H.; Tan, W. Aptamer-based microfluidic device for enrichment, sorting, and detection of multiple cancer cells. *Anal. Chem.* **2009**, *81*, 7436–7442.
18. Sheng, W.; Chen, T.; Kamath, R.; Xiong, X.; Tan, W.; Fan, Z. H. Aptamer-enabled efficient isolation of cancer cells from whole blood using a microfluidic device. *Anal. Chem.* **2012**, *84*, 4199–4206.
19. Gleghorn, J. P.; Pratt, E. D.; Denning, D.; Liu, H.; Bander, N. H.; Tagawa, S. T.; Nanus, D. M.; Giannakakou, P. A.; Kirby, B. J. Capture of circulating tumor cells from whole blood of prostate cancer patients using geometrically enhanced differential immunocapture (GEDI) and a prostate-specific antibody. *Lab Chip* **2010**, *10*, 27–29.
20. Adams, A. A.; Okagbare, P. I.; Feng, J.; Hupert, M. L.; Patterson, D.; Göttert, J.; McCarley, R. L.; Nikitopoulos, D.; Murphy, M. C.; Soper, S. A. Highly efficient circulating tumor cell isolation from whole blood and label-free enumeration using polymer-based microfluidics with an integrated conductivity sensor. *J. Am. Chem. Soc.* **2008**, *130*, 8633–8641.
21. Wang, S.; Wang, H.; Jiao, J.; Chen, K.-J.; Owens, G. E.; Kamei, K.-i.; Sun, J.; Sherman, D. J.; Behrenbruch, C. P.; Wu, H.; *et al*. Three-dimensional nanostructured substrates toward efficient capture of circulating tumor cells. *Angew. Chem., Int. Ed.* **2009**, *48*, 8970–8973.
22. Wang, S.; Liu, K.; Liu, J.; Yu, Z. T. F.; Xu, X.; Zhao, L.; Lee, T.; Lee, E. K.; Reiss, J.; Lee, Y.-K.; *et al*. Highly efficient capture of circulating tumor cells by using nanostructured silicon substrates with integrated chaotic micromixers. *Angew. Chem., Int. Ed.* **2011**, *50*, 3084–3088.
23. Han, W.; Allio, B. A.; Foster, D. G.; King, M. R. Nanoparticle coatings for enhanced capture of flowing cells in microtubes. *ACS Nano* **2009**, *4*, 174–180.
24. Mammen, M.; Choi, S.-K.; Whitesides, G. M. Polyvalent interactions in biological systems: implications for design and use of multivalent ligands and inhibitors. *Angew. Chem., Int. Ed.* **1998**, *37*, 2754–2794.
25. Kitov, P. I.; Sadowska, J. M.; Mulvey, G.; Armstrong, G. D.; Ling, H.; Pannu, N. S.; Read, R. J.; Bundle, D. R. Shiga-like toxins are neutralized by tailored multivalent carbohydrate ligands. *Nature* **2000**, *403*, 669–672.
26. de la Fuente, J. M.; Barrientos, A. G.; Rojas, T. C.; Rojo, J.; Cañada, J.; Fernández, A.; Penadés, S. Gold glyconanoparticles as water-soluble polyvalent models to study carbohydrate interactions. *Angew. Chem.* **2001**, *113*, 2317–2321.
27. Weissleder, R.; Kelly, K.; Sun, E. Y.; Shtatland, T.; Josephson, L. Cell-specific targeting of nanoparticles by multivalent attachment of small molecules. *Nat. Biotechnol.* **2005**, *23*, 1418–1423.
28. Fasting, C.; Schalley, C. A.; Weber, M.; Seitz, O.; Hecht, S.; Koksch, B.; Dernedde, J.; Graf, C.; Knapp, E.-W.; Haag, R.

Multivalency as a chemical organization and action principle. *Angew. Chem., Int. Ed.* **2012**, *51*, 10472–10498.

29. Massich, M. D.; Giljohann, D. A.; Schmucker, A. L.; Patel, P. C.; Mirkin, C. A. Cellular response of polyvalent oligonucleotide—gold nanoparticle conjugates. *ACS Nano* **2010**, *4*, 5641–5646.

30. Kim, Y.; Cao, Z.; Tan, W. Molecular assembly for high-performance bivalent nucleic acid inhibitor. *Proc. Natl. Acad. Sci.* **2008**, *105*, 5664–5669.

31. Zhao, W.; Cui, C. H.; Bose, S.; Guo, D.; Shen, C.; Wong, W. P.; Halvorsen, K.; Farokhzad, O. C.; Teo, G. S.; Phillips, J. A.; *et al*. Bioinspired multivalent DNA network for capture and release of cells. *Proc. Natl. Acad. Sci. U.S.A.* **2012**, *109*, 19626–19631.

32. Hong, S.; Leroueil, P. R.; Majoros, I. J.; Orr, B. G.; Baker, J. R., Jr.; Banaszak Holl, M. M. The binding avidity of a nanoparticle-based multivalent targeted drug delivery platform. *Chem. Biol.* **2007**, *14*, 107–115.

33. Myung, J. H.; Gajjar, K. A.; Saric, J.; Eddington, D. T.; Hong, S. Dendrimer-mediated multivalent binding for the enhanced capture of tumor cells. *Angew. Chem., Int. Ed.* **2011**, *50*, 11769–11772.

34. Huang, Y.-F.; Chang, H.-T.; Tan, W. Cancer cell targeting using multiple aptamers conjugated on nanorods. *Anal. Chem.* **2008**, *80*, 567–572.

35. Pavlov, V.; Xiao, Y.; Shlyahovsky, B.; Willner, I. Aptamer-functionalized Au nanoparticles for the amplified optical detection of thrombin. *J. Am. Chem. Soc.* **2004**, *126*, 11768–11769.

36. Farokhzad, O. C.; Jon, S.; Khademhosseini, A.; Tran, T.-N. T.; LaVan, D. A.; Langer, R. Nanoparticle-aptamer bioconjugates. *Cancer Res.* **2004**, *64*, 7668–7672.

37. Shangguan, D.; Li, Y.; Tang, Z.; Cao, Z. C.; Chen, H. W.; Mallikaratchy, P.; Sefah, K.; Yang, C. J.; Tan, W. Aptamers evolved from live cells as effective molecular probes for cancer study. *Proc. Natl. Acad. Sci.* **2006**, *103*, 11838–11843.

38. Keefe, A. D.; Pai, S.; Ellington, A. Aptamers as therapeutics. *Nat. Rev. Drug Discovery* **2010**, *9*, 537–550.

39. Wang, H.; Yang, R.; Yang, L.; Tan, W. Nucleic acid conjugated nanomaterials for enhanced molecular recognition. *ACS Nano* **2009**, *3*, 2451–2460.

40. Zheng, D.; Seferos, D. S.; Giljohann, D. A.; Patel, P. C.; Mirkin, C. A. Aptamer nano-flares for molecular detection in living cells. *Nano Lett.* **2009**, *9*, 3258–3261.

41. Chen, T.; Shukoor, M. I.; Wang, R.; Zhao, Z.; Yuan, Q.; Bamrungsap, S.; Xiong, X.; Tan, W. Smart multifunctional nanostructure for targeted cancer chemotherapy and magnetic resonance imaging. *ACS Nano* **2011**, *5*, 7866–7873.

42. Bamrungsap, S.; Chen, T.; Shukoor, M. I.; Chen, Z.; Sefah, K.; Chen, Y.; Tan, W. Pattern recognition of cancer cells using aptamer-conjugated magnetic nanoparticles. *ACS Nano* **2012**, *6*, 3974–3981.

43. Huang, Y.-F.; Liu, H.; Xiong, X.; Chen, Y.; Tan, W. Nanoparticle-Mediated IgE—Receptor Aggregation and Signaling in RBL Mast Cells. *J. Am. Chem. Soc.* **2009**, *131*, 17328–17334.

44. Mirkin, C. A.; Letsinger, R. L.; Mucic, R. C.; Storhoff, J. J. A DNA-based method for rationally assembling nanoparticles into macroscopic materials. *Nature* **1996**, *382*, 607–609.

45. Cutler, J. I.; Auyeung, E.; Mirkin, C. A. Spherical nucleic acids. *J. Am. Chem. Soc.* **2012**, *134*, 1376–1391.

46. Chen, W.; Weng, S.; Zhang, F.; Allen, S.; Li, X.; Bao, L.; Lam, R. H.; Macoska, J. A.; Merajver, S. D.; Fu, J. Nanoroughened surfaces for efficient capture of circulating tumor cells without using capture antibodies. *ACS Nano* **2013**, *7*, 566–575.

47. Lee, S.-K.; Kim, G.-S.; Wu, Y.; Kim, D.-J.; Lu, Y.; Kwak, M.; Han, L.; Hyung, J.-H.; Seol, J.-K.; Sander, C.; *et al*. Nanowire substrate-based laser scanning cytometry for quantitation of circulating tumor cells. *Nano Lett.* **2012**, *12*, 2697–2704.

48. Hurst, S. J.; Lytton-Jean, A. K. R.; Mirkin, C. A. Maximizing DNA loading on a range of gold nanoparticle sizes. *Anal. Chem.* **2006**, *78*, 8313–8318.

49. Tang, Z.; Shangguan, D.; Wang, K.; Shi, H.; Sefah, K.; Mallikratchy, P.; Chen, H. W.; Li, Y.; Tan, W. Selection of aptamers for molecular recognition and characterization of cancer cells. *Anal. Chem.* **2007**, *79*, 4900–4907.

50. Stroock, A. D.; Dertinger, S. K. W.; Ajdari, A.; Mezić, I.; Stone, H. A.; Whitesides, G. M. Chaotic mixer for microchannels. *Science* **2002**, *295*, 647–651.

51. Shangguan, D.; Cao, Z.; Meng, L.; Mallikaratchy, P.; Sefah, K.; Wang, H.; Li, Y.; Tan, W. Cell-specific aptamer probes for membrane protein elucidation in cancer cells. *J. Proteome Res.* **2008**, *7*, 2133–2139.

52. Cavé, H.; van der Werff ten Bosch, J.; Suciu, S.; Guidal, C.; Waterkeyn, C.; Otten, J.; Bakkus, M.; Thielemans, K.; Grandchamp, B.; Vilmer, E.; *et al*. Clinical significance of minimal residual disease in childhood acute lymphoblastic leukemia. *N. Engl. J. Med.* **1998**, *339*, 591–598.

53. Bottcher, S.; Ritgen, M.; Fischer, K.; Stilgenbauer, S.; Busch, R. M.; Fingerle-Rowson, G.; Fink, A. M.; Buhler, A.; Zenz, T.; Wenger, M. K.; *et al*. Minimal residual disease quantification is an independent predictor of progression-free and overall survival in chronic lymphocytic leukemia: a multivariate analysis from the randomized GCLLSG CLL8 trial. *J. Clin. Oncol.* **2012**, *30*, 980–988.

54. Song, Y.; Zhu, Z.; An, Y.; Zhang, W.; Zhang, H.; Liu, D.; Yu, C.; Duan, W.; Yang, C. J. Selection of DNA aptamers against epithelial cell adhesion molecule for cancer cell imaging and circulating tumor cell capture. *Anal. Chem.* **2013**, *85*, 4141–4149.

55. Lupold, S. E.; Hicke, B. J.; Lin, Y.; Coffey, D. S. Identification and characterization of nuclease-stabilized RNA molecules that bind human prostate cancer cells via the prostate-specific membrane antigen. *Cancer Res.* **2002**, *62*, 4029–4033.

56. Valencia, P. M.; Farokhzad, O. C.; Karnik, R.; Langer, R. Microfluidic technologies for accelerating the clinical translation of nanoparticles. *Nat. Nanotechnol.* **2012**, *7*, 623–629.

57. Liu, J.; Lu, Y. Preparation of aptamer-linked gold nanoparticle purple aggregates for colorimetric sensing of analytes. *Nat. Protoc.* **2006**, *1*, 246–252.

58. Zhang, X.; Servos, M. R.; Liu, J. Instantaneous and quantitative functionalization of gold nanoparticles with thiolated DNA using a pH-assisted and surfactant-free route. *J. Am. Chem. Soc.* **2012**, *134*, 7266–7269.

59. Qin, D.; Xia, Y.; Whitesides, G. M. Soft lithography for micro- and nanoscale patterning. *Nat. Protoc.* **2010**, *5*, 491–502.

60. Mata, A.; Fleischman, A. J.; Roy, S. Fabrication of multi-layer SU-8 microstructures. *J. Micromech. Microeng.* **2006**, *16*, 276.